Extreme ultra-violet movie camera for imaging microsecond time scale magnetic reconnection

Kil-Byoung Chai and Paul M. Bellan

Applied Physics, Caltech, 1200 E. California Boulevard, Pasadena, California 91125, USA

An ultra-fast extreme ultra-violet (EUV) movie camera has been developed for imaging magnetic reconnection in the Caltech spheromak/astrophysical jet experiment. The camera consists of a broadband Mo:Si multilayer mirror, a fast decaying YAG:Ce scintillator, a visible light block, and a high-speed visible light CCD camera. The camera can capture EUV images as fast as 3.3×10^6 frames per second with 0.5 cm spatial resolution. The spectral range is from 20 eV to 60 eV. EUV images reveal strong, transient, highly localized bursts of EUV radiation when magnetic reconnection occurs. © 2013 AIP Publishing LLC. [http://dx.doi.org/10.1063/1.4841915]

I. INTRODUCTION

Time-resolved fast imaging of extreme ultra-violet (EUV) and soft x-ray radiation is useful to understand magnetic reconnection, magnetohydrodynamic (MHD) activity, particle and energy transport, plasma stability, and turbulence in laboratory plasmas such as tokamaks[1–4] spheromaks,[5] reversed field pinches,[6] and stellarators.[7] Since visible light technology does not work at EUV wavelengths, conventional optical schemes based on mirrors and lenses cannot be used to collect radiation and form images. Various EUV imaging methods have been used previously, most particularly pinhole cameras[3,4,6,7] and diode arrays.[1,2,5] Pinhole cameras consist of a small pinhole to form an image, a micro-channel plate intensifier shutter that converts EUV into fast electrons, a scintillator/phosphor to convert the fast electrons into a visible light image, and a visible light camera to record the phosphor image. Pinhole cameras have the advantage of simplicity, but have extremely low sensitivity because of the necessarily small pinhole photon collection efficiency. Diode arrays have the advantage of providing good temporal resolution and three-dimensional images can be obtained from tomographic reconstruction of line-integrated diode data. However, diode arrays have low spatial resolution because cost considerations dictate that only a small number of channels are feasible.

Photon-efficient, high spatial resolution imaging at EUV wavelengths has recently become possible using multilayer mirrors. Unlike conventional silver-coated visible light mirrors, multilayer mirrors have high EUV/soft x-ray reflectivity at normal incidence to the mirror surface. Multilayer mirrors consist of alternating stacks of two different materials with half-wavelength periodicity so as to satisfy the Bragg constructive interference condition. At EUV wavelengths, the periodicity is a few nm and so multilayer mirrors are difficult to fabricate and are expensive. Multilayer mirrors are now widely used in the EUV lithography industry[8] and in spacecraft telescopes.[9–11] For example, the Atmospheric Imaging Assembly on the Solar Dynamics Observatory uses multilayer mirrors coupled to back-illuminated CCD cameras[11] to take EUV images of the sun every 12 s at several different spectral energies.

We report here an ultra-fast, multilayer-mirror-based, EUV imaging movie camera. This camera has been designed to image pulsed plasmas in a lab experiment investigating complex, dynamic plasma behavior relevant to spheromak formation, astrophysical jets, and solar corona loops.[12,13] Recent observations using filtered EUV-sensitive PIN diode detectors shown in Fig. 1 revealed two distinct strong, transient bursts of EUV radiation, ranging from 20 eV to 60 eV, that occur in association with two respective distinct fast, transient magnetic reconnection events. The characteristic duration of these EUV radiation bursts is a few μs. The highly transient nature of the EUV emission and the complex, dynamic, nature of the visible light images suggest that the EUV burst should have a well-defined localized, morphology which, if captured, would provide useful information on the reconnection process. In order to capture this image, we have developed the camera described here.

II. OPTICAL DESIGN

Figure 2(a) shows the layout of the ultra-fast EUV imaging camera system which consists of a high-speed visible camera (DRS Imacon 200), a YAG:Ce scintillator (Crytur), a Mo:Si multilayer mirror (NTT-AT), and two visible-light flat mirrors. Because EUV cannot penetrate glass and is highly attenuated in air, the entire EUV optical system is installed inside the vacuum chamber as shown in Fig. 2(b). The scintillator converts the EUV image into visible light which can then be observed from outside the vacuum chamber.

The Imacon 200 visible-light camera, capable of 2×10^8 fps, is located outside the vacuum chamber and views the image on the scintillator through a window on the vacuum chamber. The scintillator must be sufficiently fast to provide temporal resolution of the reconnection activity which has a 1 μs time scale. A YAG:Ce scintillator was selected because it has a 70 ns decay time. This scintillator converts EUV/x-ray photons into 550 nm visible photons which are then detected by the high speed visible light camera. The scintillator is in the form of crystal to provide high spatial resolution. The scintillator diameter and thickness are 25 mm and 100 μm, respectively, so that it can stand free without external support.
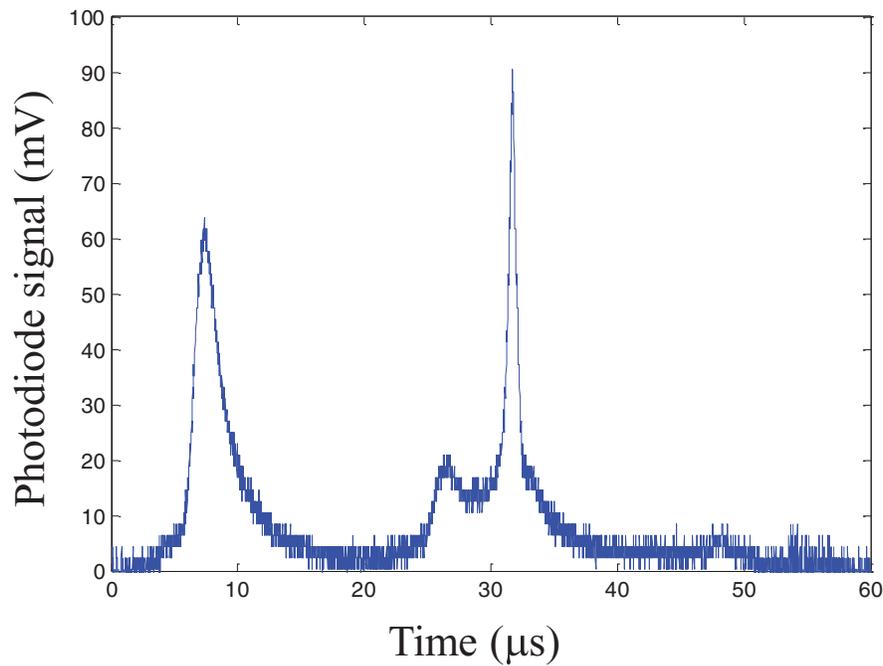
FIG. 1. Al filtered EUV-sensitive PIN diode signal. The first peak corresponds to the spider leg merging time and the second peak corresponds to the kink/Rayleigh-Taylor reconnection time.

The plasma-facing side of the scintillator is coated with a 200 nm Al film to block visible light while not severely attenuating the desired EUV photons. The transmission for 20–60 eV EUV photons is >0.6 and the visible light transmission is <10^{-5}. The conversion efficiency of the crystalline YAG:Ce scintillator for 20–60 eV EUV photons into visible photons is not known, but is presumed to be similar to the reported >1% efficiency of a YAG:Ce powder scintillator (see Fig. 4 in Ref. 14).

A broadband concave Mo:Si multilayer mirror is used to focus the EUV photons onto the YAG:Ce scintillator. This mirror was custom-fabricated by NTT-AT[15] and has alternating layers of Mo and Si periodically stacked (~18 nm) to satisfy the Bragg constructive interference condition ($n\lambda = 2d\sin\theta$ where n is integer, λ is the target wavelength, d is periodicity, and θ is the incident angle; here target wavelength = 36 nm and $\theta \sim 80^{\circ}$). The mirror diameter and focal length are 50.8 mm and 50 mm, respectively. The
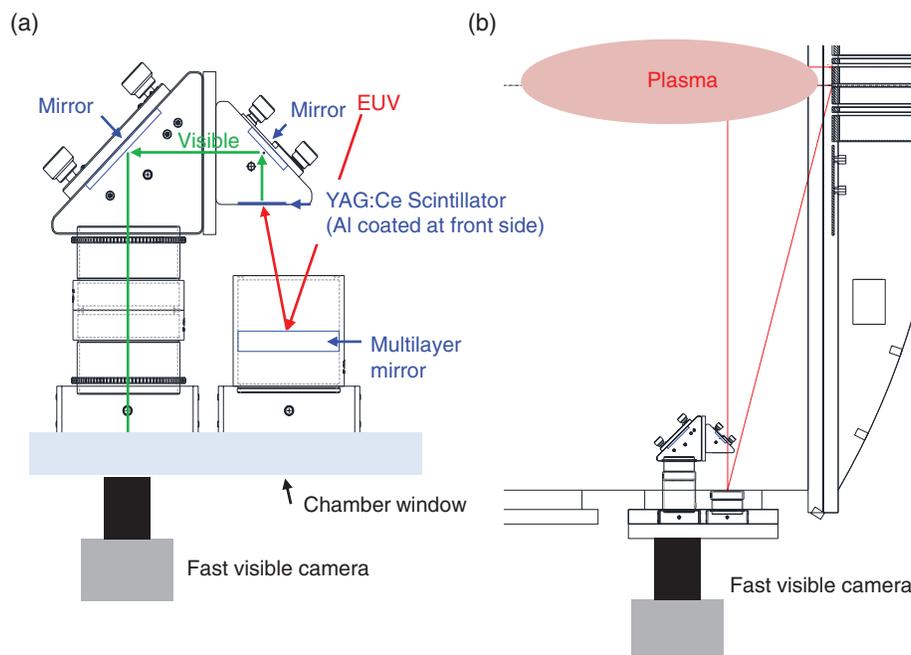

FIG. 2. (a) Sketch of ultra-fast EUV imaging diagnostic. (b) Top view of experimental layout showing EUV imaging diagnostic mounted on the first port.
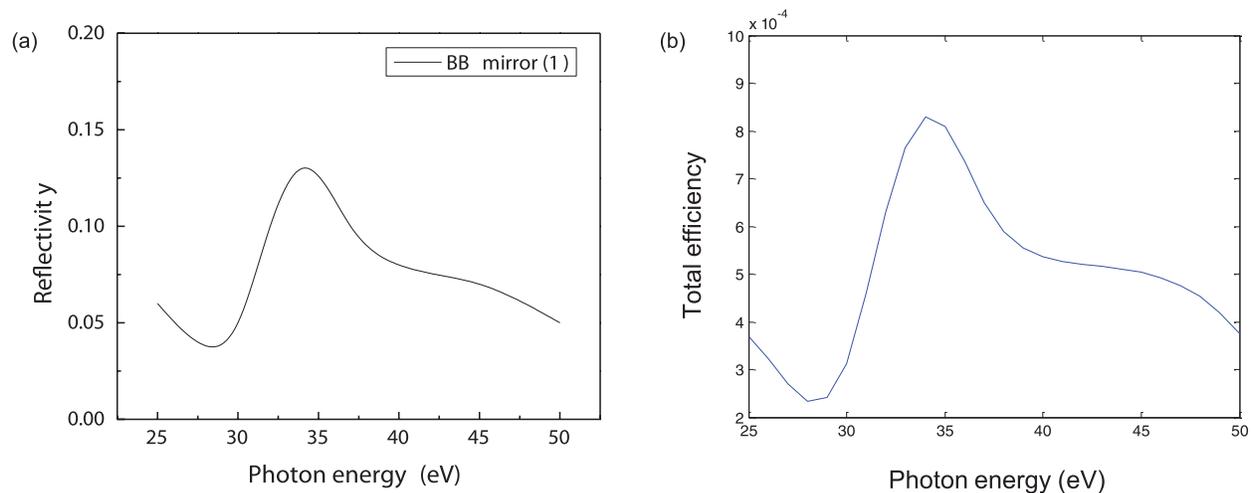
FIG. 3. (a) Reflectivity of Mo:Si multilayer mirror.[15] (b) Conversion efficiency defined as number of incoming EUV photons divided by output visible photons.

multilayer mirror reflectivity, shown in Fig. 3(a), is provided by NTT-AT[15] and has a maximum of 13% at 34 eV (36 nm) and the FWHM is approximately 5 eV. The distance between plasma and mirror is 60 cm while the distance between mirror and scintillator is 5.45 cm so the optical system provides a demagnification of 11.

The net photon conversion efficiency of the combined multilayer mirror, light blocking Al filter, and scintillator, defined as incoming EUV photons divided by output visible-light photons is shown in Fig. 3(b) and is between 5×10^{-4} and 9×10^{-4} for 30–50 eV. Filtered EUV-sensitive PIN diode detectors in the vacuum chamber indicate that the plasma emits a transient isotropic 50 kW EUV burst when magnetic reconnection occurs; this corresponds to 1.0×10^{22} photons s^{-1} assuming 30 eV energy for all EUV photons. Taking into account the solid angle subtended by the multilayer mirror and the fact that the multilayer mirror is blocked by scintillator support structure by 50%, 2.2×10^{18} photons s^{-1} will reach the mirror. Using the EUV to visible photon conversion efficiency, the number of visible light photons generated by the scintillator is 2.0×10^{15} photons s^{-1}. A substantial fraction of these visible light photons are lost because of the small solid angle subtended by the lens on the visible light camera (lens diameter: 3.57 cm, distance from scintillator: 25 cm, collection efficiency = 1.3×10^{-3}) and because of the internal camera optics (efficiency: 1.3×10^{-1}). These conversion and collection efficiencies show that there will be 3.2×10^{4} visible light photons entering the camera sensor during 100 ns exposure time. Because these photons will cover roughly $50 \times 50 = 2500$ pixels (obtained from Fig. 7(d)), one pixel can get 13 photons for 100 ns, which is sufficient to obtain meaningful images.

III. RESULTS

A. Visible light test

Before attempting to capture EUV images from an actual plasma, the spatial resolution and field of view of the EUV imaging system were tested using visible light. The

scintillator was temporally replaced by a ground glass diffuser (120 grit) to enable visible photons to travel through the entire system. The remainder of the system was unchanged from the EUV setup. A set of computer-generated phantom test objects was displayed on an LCD monitor. These phantom test objects, shown in Figs. 4(a)–4(c), were located at the same 60 cm distance from the focusing mirror as a plasma would be in an actual experiment.

Figures 4(d)–4(f) show images of these phantom objects produced by the temporary visible-light optical system. The test object in Fig. 4(d) is a grid with 25.4 mm × 25.4 mm spatial periodicity; Fig. 4(d) shows that the optical system field of view is from 0 mm to 200 mm in the horizontal direction and from −25 mm to 175 mm in the vertical direction. The vertical extent of the field of view has been intentionally arranged to cover the upper part of vacuum chamber because the plasma jet usually kinks upward. The test object in Fig. 4(e) consists of 1.27 cm diameter dots, spaced 1.27 cm from each other; Fig. 4(e) reveals that the spatial resolution of the optics is about 0.5 cm because FWHM of dots ranges between 0.4 and 0.6 cm. The test object in Fig. 4(f) is a previously
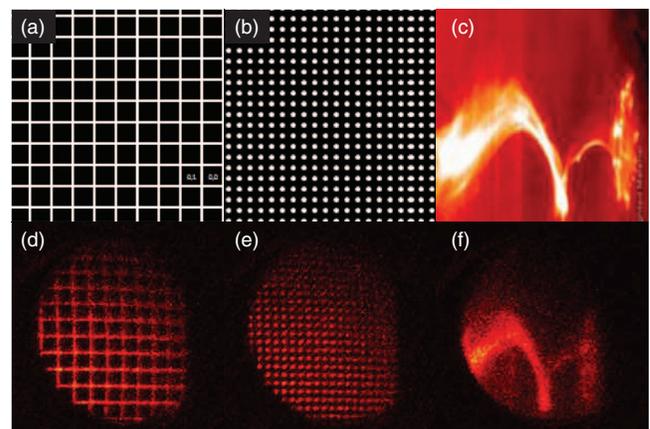

FIG. 4. (a)–(c) Phantom objects used in spatial resolution and field of view tests. These were displayed on an LCD monitor at the position where plasma would be present. (d)–(f) Images of phantom objects obtained by replacing scintillator with ground glass diffuser to achieve visible light measurement.
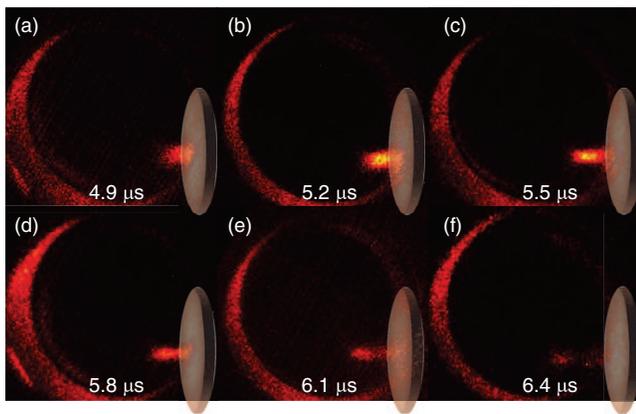
FIG. 5. EUV images from actual plasma jet. Images were captured starting at 4.9 μs with 300 ns interframe time and 100 ns exposure time. The source electrodes are located on the right side of each image as indicated by ellipse. The circular rings are visible light leakage from the perimeter of the scintillator. The jet speed is estimated to be 21 km/s.

made visible light photo of the plasma; Fig. 4(f) shows that the optical system should be able to resolve the structure of a kinked plasma jet. The spatial variation of brightness and clarity is a consequence of coma aberration caused by the light source (plasma) being substantially off the axis of the concave mirror.

B. EUV results

1. First EUV burst (spider leg merging)

Figures 5(a)–5(f) show the EUV images taken from the actual plasma jet (scintillator now back in place and EUV optics in vacuum as in Fig. 2(b)). These images were captured starting at 4.9 μs and had a 300 ns interframe time and a 100 ns exposure time. The electrode from which the jet originates is the ellipse located on the extreme lower right of each image. The large crescent on the left of each of Figs. 5(a)–5(f) is visible light leaking around the perimeter of the scintillator. The EUV image originating from the center of the electrode in each of Figs. 5(a)–5(f) brightens from 4.9 μs to 5.5 μs and then dims; during this time, this bright region moves leftwards, away from the source electrode. The size of the brightest EUV segment is about 5 cm $\times$ 3 cm. The estimated velocity of the moving EUV front is ~21 km/s (2.54 cm in 1.2 μs) in good agreement with the plasma jet velocity measured in visible light.[12] Visible light imaging shows that during this 4.9 μs to 5.5 μs interval, the inner portions of 8 initial plasma arches having morphology of a spider, merge to become a single jet.[16] This merging requires the inner parts of the "spider legs" to undergo magnetic reconnection. The EUV images are bright where this merging occurs while regions outside the merging region are dim. This EUV burst is transient, lasting only about 2 μs. The time at which this bright EUV burst occurs is in good agreement with the first transient burst observed by the separately mounted EUV diode. The time of the first peak in Fig. 1 is different from that of EUV images in Fig. 5 because they are not from the same plasma shot.
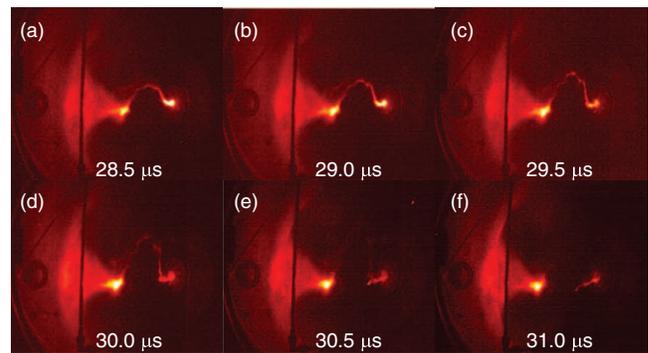

FIG. 6. Visible light images taken by Imacon camera without EUV optics at the second port of chamber (See Fig. 2(b)) from 28.5 μs with 500 ns interframe time and 20 ns exposure time. Plasma undergoes kink and Rayleigh-Taylor instabilities during this period. As a result of this instability cascade, magnetic reconnection takes place and the plasma breaks off from its source electrode. Apex of kinked structure dims as the plasma breaks off from its source electrode.

2. Second EUV burst (kink/Rayleigh-Taylor reconnection)

The merged jet propagates away from the source electrode, accelerated by MHD forces.[16] When the jet length exceeds a critical value given by the Kruskal-Shafranov criterion, the jet suddenly develops a strong kink instability[15] as shown in Fig. 6 (visible light). The lateral acceleration of the jet caused by the kink instability provides an effective gravity in the frame of the jet. This effective gravity provides the environment for a much faster growing secondary instability, namely, a Rayleigh-Taylor instability.[12] The fast-growing ripples of the Rayleigh-Taylor instability choke the jet cross-section down to a scale smaller than the ion skin depth (Figs. 6(a)–6(d)). This leads to a second and different magnetic reconnection[12] event which severs the jet from the source electrode (Figs. 6(e)–6(f)).

Figures 7(a)–7(f) are EUV images, taken during this time period but from a different shot than the visible images (from 29.4 μs to 30.9 μs with 300 ns interframe time and 100 ns exposure time). The lateral velocity of the kink instability increases from 28 km/s to 85 km/s during 29.7–30.3 μs
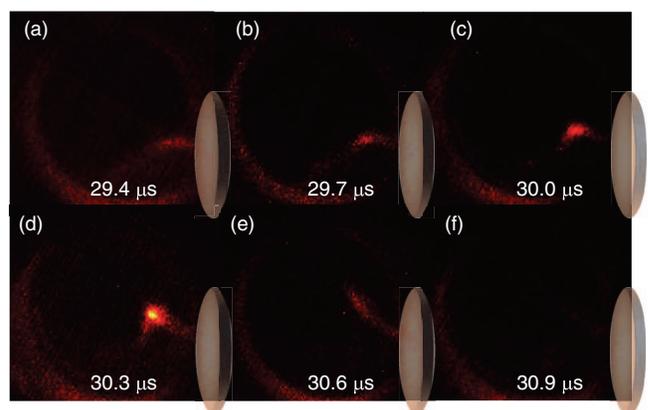

FIG. 7. EUV images starting at 29.4 μs with 300 ns interframe time and 100 ns exposure time. These images were taken from a different plasma shot than the visible images. As magnetic reconnection occurs, a strong, transient highly localized EUV burst is observed at 30.3 μs.

indicating a very large lateral acceleration ($\sim 10^{11}$ m s^{-2}). The EUV signal brightness peaks at 30.3 μs coincident with this large acceleration and appears at the apex of the kinked structure. The spatial extent of this EUV burst is extremely localized, having an area of only 2.5 cm $\times$ 2.5 cm. After the time of peak intensity, the bright EUV segment on the apex elongates vertically and then gradually disappears. The duration of this transient Rayleigh-Taylor-caused reconnection event is much less than the earlier EUV burst associated with spider leg merging.

The EUV images during this second magnetic reconnection event differ considerably from the visible light images. In the visible light images, the apex of the kinked jet dims (Fig. 6(e)) whereas the apex becomes very bright in the EUV images (Fig. 7(d)). This presumably indicates that the region where bright EUV is observed is locally hot because plasma particles are heated by magnetic reconnection. Also, the later elongation of the localized "hot spot" suggests that the heated particles move in both upper and lower directions away from the original heating location; this hot particle dynamics is not captured by the visible light images.

IV. CONCLUSION

An ultra-fast EUV imaging movie camera system has been developed which can capture EUV images as fast as 3.3×10^6 fps with 0.5 cm spatial resolution. The images provided by this camera differ substantially from visible light images when magnetic reconnection associated with the kink-driven Rayleigh-Taylor instability occurs. The extreme spatial and temporal localization of the EUV images suggests the EUV radiation results from localized heating of plasma particles by magnetic reconnection. While the temporal and spatial resolution of the camera system is adequate to resolve these EUV bursts, the camera is limited by low photon collection efficiency and by coma aberration of the multilayer mirror. The low collection efficiency could be improved by using a multilayer mirror with higher reflectivity, a higher sensitivity scintillator (LuAG:Ce scintillator improves efficiency 50%[17]), and a thinner Al light-blocking filter (100 nm film improves efficiency 33%). Each of these improvements could increase sensitivity by few tens of percent so if the camera were optimized by these means, the overall camera performance would increase by a factor of the order 2–5. On the other hand, if the camera lens system were to be replaced by an optical fiber imaging bundle system with one face at the scintillator, sensitivity could be improved by two orders of magnitude. Eliminating or reducing coma aberration could be accomplished by either a computer reconstruction method or by adopting coma-free optics such as Schwarzschild optics.[18] Moving the scintillator to the axis of the multilayer mirror would decrease light efficiency by blocking more of the mirror, but would reduce coma aberration significantly. We are now investigating upgrading of the camera using a combination of these methods.

The camera design could be modified to measure higher energy photons (soft x-ray) by using a multilayer mirror designed for higher energies. Since scintillator efficiency increases with incident photon energy,[14] it is expected that better images would be obtained for soft x-rays than for EUV.

[1] G. A. Bobrovskij, D. A. Kislov, E. S. Lyadina, and P. V. Savrukhin, Rev. Sci. Instrum. **62**, 886 (1991).
[2] B. Alper *et al.*, Rev. Sci. Instrum. **68**, 778 (1997).
[3] S. von Goeler *et al.*, Rev. Sci. Instrum. **70**, 599 (1999).
[4] B. C. Stratton *et al.*, Rev. Sci. Instrum. **75**, 3959 (2004).
[5] A. E. Askren *et al.*, *46th Annual meeting of the Division of Plasma Physics, Savannah, GA, USA, 15–19 November 2004* (American Physics Society, 2004).
[6] T. Onchi *et al.*, Rev. Sci. Instrum. **81**, 073502 (2010).
[7] S. Ohdachi, K. Toi, G. Fuchs, S. von Goeler, and S. Yamamoto, Rev. Sci. Instrum. **74**, 2136 (2003).
[8] S. Bajt *et al.*, Opt. Eng. **41**, 1797 (2002).
[9] J.-P. Delaboudiniere *et al.*, Solar Phys. **162**, 291 (1995).
[10] J. K. Culhane *et al.*, Sol. Phys. **243**, 19 (2007).
[11] J. R. Lemen *et al.*, Sol. Phys. **275**, 17 (2012).
[12] A. L. Moser and P. M. Bellan, Nature (London) **482**, 379 (2012).
[13] E. V. Stenson and P. M. Bellan, Phys. Rev. Lett. **109**, 075001 (2012).
[14] A. Baciero *et al.*, J. Synchrotron Radiat. **7**, 215 (2000).
[15] Multilayer mirror custom fabricated by NTT-AT, Shinjuku Mitsui Building 2-1-1, Nishi-shinjuku, Shinjuku-ku, Tokyo 163-0431, Japan.
[16] D. Kumar and P. M. Bellan, Phys. Rev. Lett. **103**, 105003 (2009).
[17] J. Tous, M. Horvath, L. Pina, K. Blazek, and B. Sopko, Nucl. Instrum. Methods Phys. Res. A **591**, 264 (2008).
[18] K. Schwarzschild, Abh. Wiss. Gottingen **10**, 4 (1905).